Non-Franck–Condon effects in photoionization of the 3 3Π Rydberg state of NH

Kwanghsi Wang, J. A. Stephens, and V. McKoy

Citation: The Journal of Chemical Physics **93**, 7874 (1990); doi: 10.1063/1.459369
View online: http://dx.doi.org/10.1063/1.459369
View Table of Contents: http://scitation.aip.org/content/aip/journal/jcp/93/11?ver=pdfcov
Published by the AIP Publishing

Non-Franck–Condon effects in photoionization of the 3 $^3\Pi$ Rydberg state of NH

Kwanghsi Wang, J. A. Stephens, and V. McKoy
Arthur Amos Noyes Laboratory of Chemical Physics,[a] *California Institute of Technology, Pasadena, California 91125*

(Received 16 July 1990; accepted 29 August 1990)

Strong non-Franck–Condon behavior is predicted to occur in the vibrationally resolved photoionization spectra of NH for (3 + 1) resonance enhanced multiphoton ionization processes via the 3 $^3\Pi$ Rydberg state. The non-Franck–Condon effects are interpreted on the basis of rapid orbital evolution, Cooper minima, and internuclear distance dependence of the dipole transition moment and cross sections. A Cooper minimum occurs in the $5\sigma \rightarrow k\pi$ channel at small internuclear distances, where NH resembles its united atom, oxygen. The iterative Schwinger variational method and multiplet-specific ion potentials are employed in the calculation of the photoelectron continuum wave functions. Cross sections and asymmetry parameters for photoionization of the NH ground state leading to the $X\,^2\Pi$, $a\,^4\Sigma^-$, and $A\,^2\Sigma^-$ ions are also reported.

I. INTRODUCTION

Resonance enhanced multiphoton ionization (REMPI) coupled with high-resolution photoelectron spectroscopy is a powerful probe of atomic and molecular excited states and their photoionization dynamics.[1-5] The use of REMPI techniques can be expected to yield significant new information on the electronic structure and photoionization dynamics of small radicals. NH was the first transient radical to be probed with this technique, via a (3 + 1) scheme from the $a\,^1\Delta$ state.[6] The spectroscopy of NH has also recently received attention through photodissociation studies of NH_3,[7] HN_3,[8] and NHCO,[9] of collisions of hydrogen and azide radical N_3,[10] and in combustion processes.[11] Photoionization and photodissociation processes of NH, as well as the recombination of NH^+, are also important in predicting the abundance of precursors such as NH_3 and HN_3 in interstellar clouds.[12-14] However, little is actually known about the details of the photoionization and photodissociation processes of NH itself. In this paper, we study the vibrationally resolved photoionization dynamics of the 3 $^3\Pi(1\pi 3p\sigma)$ Rydberg state of NH. Of particular interest is the understanding and further study of non-Franck–Condon effects induced by rapid orbital evolution and Cooper minima, previously predicted for (3 + 1) REMPI of OH via the $D\,^2\Sigma^-(1\pi^2 3p\sigma)$ Rydberg state.[15] Such rapid Rydberg orbital evolution in hydrides has also been recently predicted to have a significant influence on the rotational distributions of molecular ions, specifically for REMPI of CH via the $E'\,^2\Sigma^+(3p\sigma)$ state.[16] In the present paper, we also report results for ground state photoionization of NH leading to the $X\,^2\Pi$, $a\,^4\Sigma^-$, and $A\,^2\Sigma^-$ molecular ions.

An outline of the paper is as follows: In Sec. II, we discuss some details of the multiplet-specific calculations for photoionization of both the Rydberg and ground states. In Sec. III, results and discussions are presented, followed by a brief conclusion in Sec. IV.

[a] Contribution No. 8173.

II. THEORY

A. Multiplet-specific wave functions and potentials

NH is an open shell molecule with the ground state electronic configuration $1\sigma^2 2\sigma^2 3\sigma^2 1\pi^2\, X\,^3\Sigma^-$. Ionization of a 3σ electron results in the $a\,^4\Sigma^-$ and $A\,^2\Sigma^-$ ionic states, while ionization of a 1π electron leads to the $X\,^2\Pi$ ionic state. The 3 $^3\Pi$ Rydberg state results from excitation of a 1π electron to the 5σ orbital. The 5σ orbital is the second member of a Rydberg series converging to the $NH^+\,X\,^2\Pi$ ion and in the united atom designation is denoted "$3p\sigma$."

Within the frozen core Hartree–Fock approximation assumed here, there are four dipole-allowed transition channels for photoionization of the 5σ electron of the 3 $^3\Pi$ Rydberg state. The electronic continuum wave functions are

$$\Psi(^3\Pi) = |(\text{core})1\pi_+ k\sigma|, \tag{1a}$$

$$\Psi(^3\Delta) = |(\text{core})1\pi_+ k\pi_+|, \tag{1b}$$

$$\Psi(^3\Sigma^-) = \frac{1}{\sqrt{2}}[|(\text{core})1\pi_+ k\pi_-| - |(\text{core})1\pi_- k\pi_+|], \tag{1c}$$

and

$$\Psi(^3\Sigma^+) = \frac{1}{\sqrt{2}}[|(\text{core})1\pi_+ k\pi_-| + |(\text{core})1\pi_- k\pi_+|], \tag{1d}$$

where (core) $= 1\sigma^2 2\sigma^2 3\sigma^2$. With these wave functions, the static-exchange, one-particle Schrödinger equations for the photoelectron orbital ϕ_k can be obtained[17,18] from the variational expression $\langle \delta\Psi | H - E | \Psi \rangle = 0$, where H is the fixed-nuclei Hamiltonian and E is the total energy. They are of the form

$$P\left[f + \sum_{\text{core}} (2J_i - K_i) + a_n J_n + b_n K_n + \alpha S''_{1\pi} + \beta S'_{1\pi} - \epsilon | P \rangle \phi_k\right] = 0, \tag{2}$$

 0021-9606/90/237874-09$03.00

where J_i and K_i are the Coulomb and exchange operators, respectively, and P is a projection operator which enforces orthogonality of the continuum orbital to the occupied orbitals.[17,18] The photoelectron kinetic energy is given by $\epsilon = \frac{1}{2}k^2$. The operators S'' and S' are defined by

$$S''_\pi \phi_+(\mathbf{r}_1) = \phi_-(\mathbf{r}_1) \int d^3\mathbf{r}_2 [\pi_-(\mathbf{r}_2)]^* \frac{1}{r_{12}} \pi_+(\mathbf{r}_2) \tag{3}$$

and

$$S'_\pi \phi_+(\mathbf{r}_1) = \pi_+(\mathbf{r}_1) \int d^3\mathbf{r}_2 [\pi_-(\mathbf{r}_2)]^* \frac{1}{r_{12}} \phi_-(\mathbf{r}_2). \tag{4}$$

The one-electron operator in Eq. (2) is

$$f = -\frac{1}{2}\nabla_i^2 - \sum_\alpha \frac{Z_\alpha}{r_{i\alpha}}, \tag{5}$$

where Z_α is a nuclear charge. Using the wave functions of Eq. (1), the coefficients a_n, b_n, α, and β are summarized in Table I.

With the same approximations, the continuum wave functions for ground state photoionization are also readily established. The ejection of an electron from the 1π orbital yields the $X\,^2\Pi$ ionic state with an ionization potential of 13.50 eV.[19,20] The dipole-allowed final state continuum wave functions are

$$\Psi(^3\Sigma^-) = \frac{1}{\sqrt{2}}[|(\text{core})1\pi_+ k\pi_-| - |(\text{core})1\pi_- k\pi_+|], \tag{6a}$$

$$\Psi(^3\Pi) = |(\text{core})1\pi_+ k\sigma|, \tag{6b}$$

and

$$\Psi(^3\Pi) = |(\text{core})1\pi_- k\delta_+| \tag{6c}$$

with (core) $= 1\sigma^2 2\sigma^2 3\sigma^2$. The removal of an electron from the 3σ orbital of NH produces the $a\,^4\Sigma^-$ and $A\,^2\Sigma^-$ ionic states, with ionization potentials of 13.54 and 16.17 eV,[20,21] respectively. The final state continuum wave functions resulting from photoionization of the 3σ orbital leading to the $a\,^4\Sigma^-$ ion are

$$\Psi(^3\Sigma^-) = \frac{1}{\sqrt{12}}[|3(\text{core})3\sigma 1\pi_+ 1\pi_- \overline{k\sigma}| - |(\text{core})3\sigma 1\pi_+ \overline{1\pi}_- k\sigma| - |(\text{core})3\sigma \overline{1\pi}_+ 1\pi_- k\sigma| - |(\text{core})\overline{3\sigma}1\pi_+ 1\pi_- k\sigma|] \tag{7a}$$

and

$$\Psi(^3\Pi) = \frac{1}{\sqrt{12}}[3|(\text{core})3\sigma 1\pi_+ 1\pi_- \overline{k\pi}_+| - |(\text{core})3\sigma 1\pi_+ \overline{1\pi}_- k\pi_+| - |(\text{core})3\sigma \overline{1\pi}_+ 1\pi_- k\pi_+| - |(\text{core})\overline{3\sigma}1\pi_+ 1\pi_- k\pi_+|] \tag{7b}$$

with (core) $= 1\sigma^2 2\sigma^2$. The final state continuum wave functions for photoionization of the 3σ orbital leading to the $A\,^2\Sigma^-$ ion are

$$\Psi(^3\Sigma^-) = \frac{1}{\sqrt{6}}[2|(\text{core})\overline{3\sigma}1\pi_+ 1\pi_- k\sigma| - |(\text{core})3\sigma \overline{1\pi}_+ 1\pi_- k\sigma| - |(\text{core})3\sigma 1\pi_+ \overline{1\pi}_- k\sigma|] \tag{8a}$$

and

$$\Psi(^3\Pi) = \frac{1}{\sqrt{6}}[2|(\text{core})\overline{3\sigma}1\pi_+ 1\pi_- k\pi_+| - |(\text{core})3\sigma \overline{1\pi}_+ 1\pi_- k\pi_+| - |(\text{core})3\sigma 1\pi_+ \overline{1\pi}_- k\pi_+|] \tag{8b}$$

with (core) $= 1\sigma^2 2\sigma^2$. The one-electron equations for the photoelectron orbitals have the general form of Eq. (2). Their coefficients are summarized in Table II. The coefficients for the $a\,^4\Sigma^-$ and $A\,^2\Sigma^-$ ions are identical to those for $3\sigma_g$ photoionization of O_2.[22] It is worth noting that the first excited state $a\,^4\Sigma^-$ of NH^+ lies only 354 cm^{-1} above its ground state $X\,^2\Pi$,[23] while for the isoelectronic molecule CH, there is a 7660 cm^{-1} energy difference between its first excited state $a\,^4\Sigma^-$ and ground state $X\,^2\Pi$.[19]

TABLE I. Coefficients of the static-exchange potential in Eq. (2) for NH 3 $^3\Pi$ Rydberg state photoionization.

		a_n/b_n			α/β
Ion	Channel[a]	5σ	$1\pi_+$	$1\pi_-$	
$X\,^2\Pi$	$^3\Pi$	0/0	1/−1	0/0	0/0
	$^3\Delta$	0/0	1/−1	0/0	0/0
	$^3\Sigma^-$	0/0	1/−1	0/0	−1/1
	$^3\Sigma^+$	0/0	1/−1	0/0	1/−1

[a] Channel designates symmetry of the ion plus photoelectron system.

TABLE II. Coefficients of the static-exchange potential in Eq. (2) for NH ground state photoionization.

Ion	Channel[a]	a_n/b_n			α/β
		3σ	$1\pi_+$	$1\pi_-$	
$a\,^4\Sigma^-$	$^3\Sigma^-$	$1/\frac{1}{3}$	$1/\frac{1}{3}$	$1/\frac{1}{3}$	0/0
	$^3\Pi$	$1/\frac{1}{3}$	$1/\frac{1}{3}$	$1/\frac{1}{3}$	0/0
$A\,^2\Sigma^-$	$^3\Sigma^-$	$1/-\frac{1}{3}$	$1/-\frac{5}{6}$	$1/-\frac{5}{6}$	0/0
	$^3\Pi$	$1/-\frac{1}{3}$	$1/-\frac{5}{6}$	$1/-\frac{5}{6}$	0/0
$X\,^2\Pi$	$^3\Sigma^-$	$2/-1$	$1/-1$	0/0	$-1/1$
	$^3\Pi$	$2/-1$	$1/-1$	0/0	0/0
	$^3\Pi$	$2/-1$	0/0	$1/-1$	0/0

[a] Channel designates symmetry of the ion plus photoelectron system.

B. Numerical details

To obtain the photoelectron orbitals, we have used an iterative procedure, based on the Schwinger variational principle,[17,18] to solve the Lippmann–Schwinger equations associated with Eq. (2). In this procedure, the static-exchange potential is approximated by a separable form

$$U(\mathbf{r},\mathbf{r}') = \sum_{i,j} \langle \mathbf{r}|U|\alpha_i\rangle (U^{-1})_{ij} \langle \alpha_j|U|\mathbf{r}'\rangle, \qquad (9)$$

where the matrix U^{-1} is the inverse of the matrix with elements $(U)_{ij} = \langle \alpha_i|U|\alpha_j\rangle$ and the α's are discrete basis functions such as Cartesian or spherical Gaussian functions. U is twice the static-exchange potential in Eq. (2) with the long-range Coulomb potential removed. Converged solutions of the Lippmann–Schwinger equations with this separable potential can be obtained iteratively. In this study, two iterations provided converged solutions of Eq. (2). The basis sets used in the expansion of Eq. (9) are given in Table III.

The ground state self-consistent field (SCF) wave function for NH was obtained with a $(9s5p2d/4s3p2d)$ basis of contracted Cartesian Gaussian functions.[24] At the equilibrium internuclear distance of $R_e = 1.9616$ bohr, the total SCF energy with this basis is -54.9697 a.u. We used the improved-virtual-orbital (IVO) method[25] to obtain the wave function of the resonant Rydberg state. This IVO basis was augmented with five s- and p-type diffuse functions (with exponents 0.05, 0.03, 0.01, 0.005, and 0.001) on the center-of-mass.

In these calculations, all matrix elements and functions were evaluated by employing single-center expansions about the center-of-mass. For converged results, the following parameters were used:

(i) a maximum partial wave of the photoelectron continuum orbital = 9;

TABLE III. Basis sets used in the separable potential [Eq. (9)].

Symmetry	Center	Type of Gaussian function[a]	Exponents
σ	N	Cartesian s	16.0,8.0,4.0,2.0,1.0,0.5
		z	1.0,0.5
	c.m.	Spherical $l=0$	2.0,1.0,0.5
		$l=1$	4.0,2.0,1.0,0.5
		$l=2$	2.0,1.0,0.5
		$l=3$	4.0,2.0,1.0,0.5
	H	Cartesian s	1.2,0.4,0.1
		z	1.2,0.4,0.1
π	N	Cartesian x	8.0,4.0,2.0,1.0,0.5
		xz	1.0,0.5
	c.m.	Spherical $l=1$	1.0
		$l=2$	1.0
		$l=3$	1.0
		$l=4$	1.0
	H	Cartesian x	1.2,0.4,0.1
		xz	1.2,0.4,0.1
δ	N	Cartesian xy	8.0,4.0,2.0,1.0,0.5,0.25
	c.m.	Spherical $l=2$	1.0
		$l=3$	1.0
		$l=4$	1.0
	H	Cartesian xy	1.2,0.4,0.1

[a] Cartesian Gaussian basis functions are defined as $\phi^{\alpha,l,m,n,A}(\mathbf{r}) = N(X-A_x)^l(y-A_y)^m(z-A_z)^n \times \exp(-\alpha|\mathbf{r}-\mathbf{A}^2)$ and spherical Gaussian functions are defined as $\phi^{\alpha,l,m,A}(\mathbf{r}) = N|\mathbf{r}-\mathbf{A}|^l \times \exp(-\alpha|\mathbf{r}-\mathbf{A}|^2)Y_{lm}(\Omega_{\mathbf{r}-\mathbf{A}})$, with N the normalization constant.

(ii) a maximum partial wave expansion of bound orbitals in the direct potential = 60;

(iii) a maximum partial wave expansion of 1σ, 2σ, 3σ, and 1π bound orbitals in the exchange potential = 30, 20, 15, and 15, respectively;

(iv) a maximum partial wave expansion of $1/r_{12}$ in the direct and exchange terms = 60 and 30, respectively;

(v) a maximum partial wave expansion of the nuclear potential = 60.

The Gaussian basis sets used in the representation of the static-exchange potential [Eq. (9)] included the Cartesian Gaussian functions centered on the nuclei and spherical Gaussian functions centered on the center of mass. These functions are listed in Table III. The radial integration grid extended to 60 a.u. and contained 500 points. The integration step sizes ranged from 0.01 to 0.4 up to 5 a.u., and up to 0.4 a.u. beyond this point.

The present study requires potential energy curves of the $3\,^3\Pi$ Rydberg state of NH and the $X\,^2\Pi$ state of NH^+. There are many accurate potential curves for the NH ground state and some excited states,[26-28] but few for NH^+.[19] The $3\,^3\Pi$ Rydberg state potential energy curve of Goldfield and Kirby[26] is distorted at $\sim 3.5a_0$ due to an apparent avoided crossing with a higher level. Since we are presently treating the resonant and final states at the Hartree–Fock level only, use of our potential curves with accurate equilibrium internuclear distances ($R_e = 2.11a_0$ for the Rydberg potential curve and $R_e = 2.043a_0$ for the ion potential curve)[19,26-28] is consistent with the present level of approximation. The vibrational wave functions for the $3\,^3\Pi$ Rydberg state of NH and the $X\,^2\Pi$ ground state of NH^+ were obtained by numerical integration over a range of $1.25 \leqslant R \leqslant 3.5a_0$. We used the potential curves obtained from our SCF calculations on NH^+ and the IVO calculation for NH, with R_e values slightly shifted to those quoted above. The calculated Franck–Condon factors, as well as our calculated cross sections and asymmetry parameters (discussed below), are available from the authors upon request.

III. RESULTS AND DISCUSSION

A. Photoionization of the $3\,^3\Pi$ Rydberg state

In Fig. 1, we show potential energy curves for the $X\,^3\Sigma^-(1\pi^2)$ ground state of NH, the $X\,^2\Pi(1\pi)$ state of NH^+, and a set of Rydberg states for the electronic configurations $^3\Pi$ ($1\pi n\sigma$ $n = 4$–6, solid curves) and $^3\Sigma^-$ ($1\pi m\pi$, $m = 2$–4, dashed curves) converging to the ion. As discussed in Sec. II, all of the potential energy curves were obtained from our SCF and IVO calculations. A proposed (3 + 1) REMPI scheme via the $3\,^3\Pi(1\pi 3p\sigma)$ Rydberg state is also shown and some states of the united atom oxygen and separated atoms are correlated with states of neutral NH.[29,30] The first "$3s\sigma$" member mixes strongly with the $2p_{zN}$–$1s_H$ antibonding orbital, resulting in a repulsive potential curve. This is a common feature of first-row diatomic hydrides.[31-33] Note that the $3\,^3\Pi(1\pi 3p\sigma)$ Rydberg state dissociates into the separated atoms $N(2p^23s) + H(1s)$, so that we can expect evolution of the Rydberg $3p\sigma$ orbital to nearly a nitrogen ($3s$) orbital as the molecule proceeds from the united to separated atoms. To show the rate of this change quantitatively, the angular composition of the 5σ Rydberg orbital and the total energy of this state are summarized in Table IV for various internuclear distances. It is clear that p

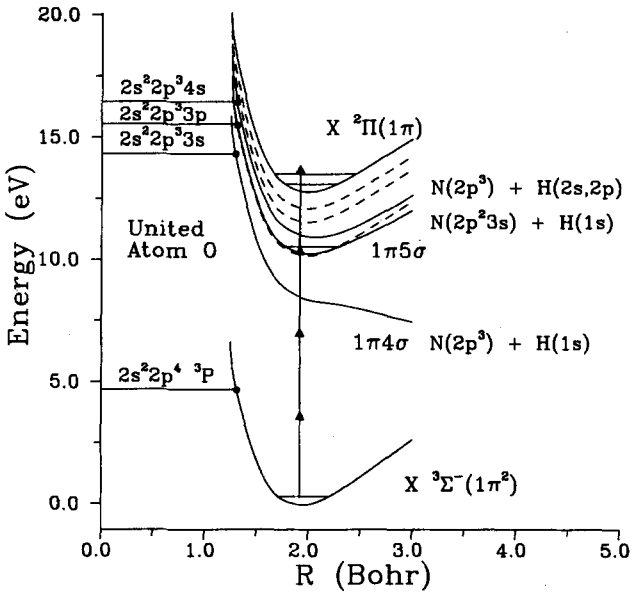

FIG. 1. Potential energy curves for the ground and first ionic states of NH and the excited states of the electronic configurations $1\pi n\sigma$ ($n = 4$–6) (solid curves) and $1\pi m\pi$ ($m = 2$–4) (dashed curves). See the text for an explanation.

TABLE IV. Total energies of the NH $3\,^3\Pi$ Rydberg state and principal angular momentum composition of the 5σ Rydberg orbital.

R(a.u.)	$-E_{total}$ (a.u.)	s(%)	p(%)	d(%)	f(%)
1.25	54.3292	13.15	86.66	0.08	0.00
1.50	54.5140	12.65	87.17	0.17	0.01
1.75	54.5807	14.08	85.47	0.44	0.06
1.9616	54.5945	18.67	80.17	1.10	0.06
2.15	54.5912	29.01	68.05	2.71	0.19
2.25	54.5865	38.41	56.91	4.24	0.35
2.50	54.5707	65.56	24.98	8.18	0.93
2.75	54.5509	79.71	9.93	8.53	1.26
3.00	54.5290	85.10	5.22	7.55	1.40
3.50	54.4866	87.58	3.69	5.99	1.68

character is dominant at smaller R and s character is dominant at larger R. These results are similar to that of the "$3p$" Rydberg states of OH and CH molecules.[15,16] As seen in Table IV, the angular momentum composition changes rapidly as the internuclear distance varies. Accompanying the rapid variation in angular momentum composition, the nodal structure of $n\sigma$ orbitals also changes and therefore significantly influences the photoionization dynamics as R varies. These properties are crucial for excited state photoionization of the diatomic hydrides. They result in a prediction of significant non-Franck–Condon effects in ion vibrational distributions, as discussed below and in our accompanying paper on OH.[34] The orbital composition remains nearly unchanged for the $n\pi$ Rydberg orbitals, i.e., they remain $\sim 99\%$ p character at all internuclear distances used in this study. This is also reflected in the nearly R-independent quantum defect functions (not shown) for these states.[35]

In Figs. 2 and 3, we show photoionization cross sections and photoelectron angular distributions (asymmetry parameter β) for photoionization of the $3\,^3\Pi(1\pi 3p\sigma)$ state of NH, leading to the $X\,^2\Pi$ ion at several internuclear distances. Due to the orbital evolution and the Cooper minimum (discussed below), the electronic transition moment (cross section) is strongly dependent on internuclear distance, and hence a simple Franck–Condon description of the vibrational branching ratios becomes invalid. A prominent result in Fig. 2 is the existence of a minimum in the cross sections at lower photon energy, and smaller internuclear distances, for $\sim R \leqslant R_e$. This is due to a Cooper zero in the electronic transition moment to the continuum final state.[36–41] The asymmetry parameters in Fig. 3 also vary rapidly with energy about a Cooper minimum.[38–41] To examine the origin of this minimum in more detail, in Fig. 4 we plot the (incoming-wave normalized) partial-wave dipole strengths $|D_l^{(-)}|^2$ as a function of photoelectron kinetic energy, for photoionization channels $5\sigma \rightarrow k\pi$ [Figs. 4(a) and 4(b)] and $5\sigma \rightarrow k\sigma$ [Figs. 4(c) and 4(d)] at $R = 1.9616$ and $2.75a_0$. In Fig. 4 (a), a Cooper minimum, which is due to a sign change in the d-wave component through the minimum, is clearly seen at low kinetic energy and around the equilibrium internuclear distance. The minimum of cross section is caused by the Cooper minimum via the $5\sigma \rightarrow k\pi$ channel only. The 5σ orbital is predominantly a $3p$ wave at small R (see Table IV). The single node in the $3p$ component of the Rydberg radial wave function ensures a large amplitude extending ~ 5–$10a_0$ from the origin. As the photoelectron energy increases, a node of the d-wave continuum moves through the outermost loop of the $3p$ wave function, resulting in a cancellation in the dipole matrix element. This is similar to the $5\sigma \rightarrow k\pi$ minimum found in $D\,^2\Sigma^-$ photoionization of OH,[15] except that it appears more pronounced in NH. Both are similar to atomic $3p \rightarrow kd$ Cooper minima observed in ground state photoionization of rare gas atoms,[36,37,41] except that for *excited states*, they occur at much lower kinetic energy due to the outward displacement of the radial node compared with a ground state $3p$ orbital. Such properties of Cooper minima have been predicted for the excited-state photoionization of heavier atoms.[38,39]

The strong internuclear distance dependence of the Rydberg-continuum transition moment, resulting from the combined effects of orbital evolution and Cooper minima,

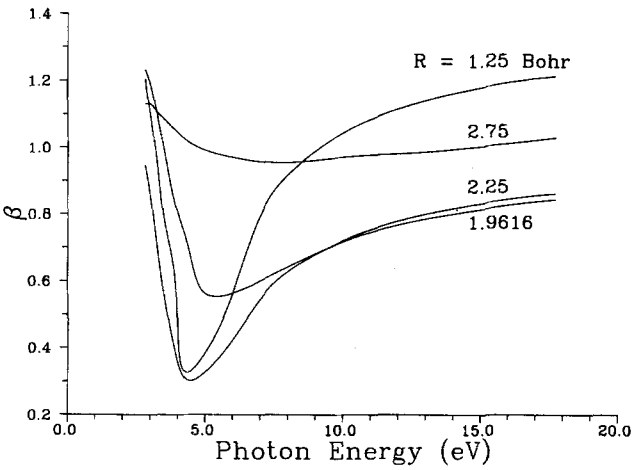

FIG. 3. Calculated (velocity form) asymmetry parameters β at various internuclear distances.

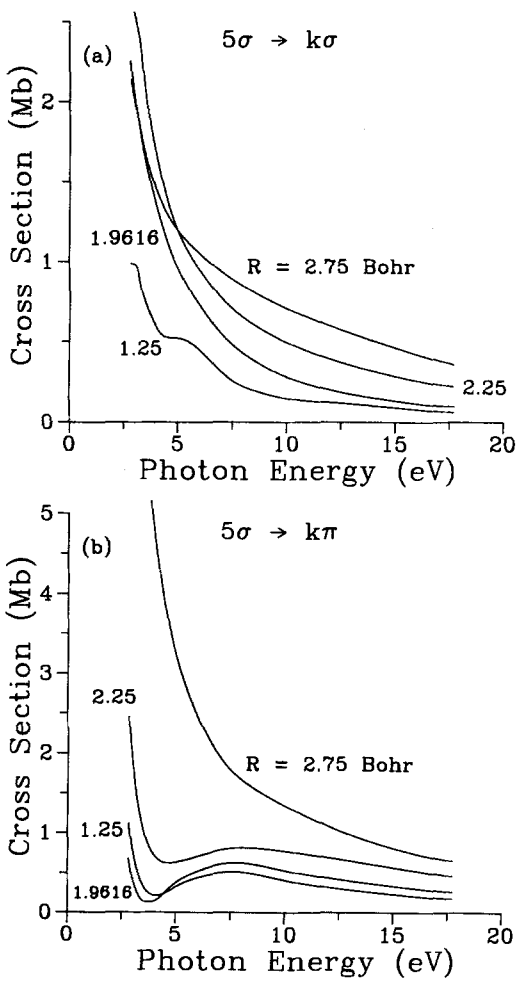

FIG. 2. Calculated (velocity form) photoionization cross sections for $5\sigma \rightarrow k\pi$ and $5\sigma \rightarrow k\sigma$ channels at various internuclear distances. The cross sections assume an ionization potential of 2.72 eV.

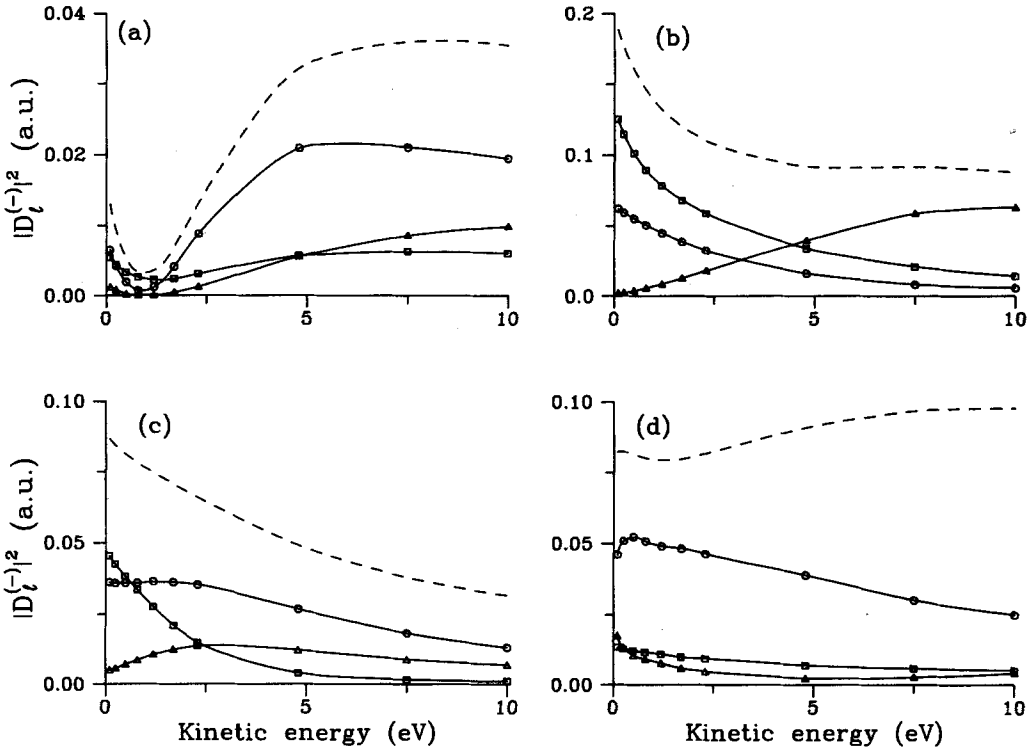

FIG. 4. Calculated dipole strengths (incoming-wave normalized, velocity form) for (a) $5\sigma \rightarrow k\pi$, $R = 1.9616a_0$; (b) $5\sigma \rightarrow k\pi$, $R = 2.75a_0$; (c) $5\sigma \rightarrow k\sigma$, $R = 1.9616a_0$; and (d) $5\sigma \rightarrow k\sigma$, $R = 2.75a_0$. In (a) and (b), the designations are: squares, $l = 1$; circles, $l = 2$; and triangles, $l = 3$. In (c) and (d), the designations are: squares, $l = 0$; circles, $l = 1$; and triangles, $l = 2$. Dashed curves in each frame give the total sum of all partial waves.

implies a breakdown of the Franck–Condon approximation to the effective vibronic transition moment. In the adiabatic-nuclei approximation, the vibrationally resolved cross sections and asymmetry parameters for a transition from the v' vibrational level to v^+ vibrational state are given by[42–44]

$$\sigma_{v'v^+}^{L,V} = \frac{4\pi^2}{3c} E \sum_{lm\mu} |\langle \chi(v^+) | I_{lm\mu}^{L,V} | \chi(v') \rangle|^2 \tag{10}$$

and

$$\frac{d\sigma_{v'v^+}^{L,V}}{d\Omega_{\hat{k}}} = \frac{\sigma_{v'v^+}^{L,V}}{4\pi} [1 + \beta_{v'v^+}^{L,V} P_2 (\cos\theta)], \tag{11}$$

where $I_{lm\mu}^{L,V}$ are partial-wave components of the length (L) or velocity (V) incoming-wave normalized transition moment. Here E is the photon energy, c is the speed of light, $\chi(v')$ and $\chi(v^+)$ are the vibrational wave functions of the Rydberg state and the ion, respectively, θ is the angle between the direction of the light polarization and photoelectron momentum $\mathbf{k}$, and P_2 is a Legendre polynomial. The Rydberg state and photoelectron orbital for the $5\sigma \rightarrow k\sigma$ and $5\sigma \rightarrow k\pi$ continuum channels were obtained over a range of internuclear distances (see column one of Table IV). We calculated vibrationally resolved cross sections $\sigma_{v'v^+}^{L,V}$ and photoelectron asymmetry parameters $\beta_{v'v^+}^{L,V}$ for one-color, $(n+1)$-REMPI processes with $n = 1$, 2, and 3. Here we show results for the $(3+1)$-REMPI process. In this case, the one-photon energies are 3.593, 3.712, 3.826, and 3.936 eV corresponding to $v' = 0$, 1, 2, and 3, respectively. We have not included alignment effects induced by the three-photon absorption in these calculations. These will be included and discussed in studies which investigate rotationally resolved REMPI of NH, OH, and CH.[45,46]

The vibrational branching ratios for $(3+1)$ REMPI as well as the Franck–Condon factors are plotted in Fig. 5, with a normalization such that a sum over branching ratios of v^+ for each level v' gives unity. Some important features displayed in Fig. 5 are: (i) the Franck–Condon approximation breaks down even for $\Delta v = v^+ - v' = 0$ when $v' \neq 0$; (ii) the maximum component shifts to $\Delta v = 1$ in larger v'; (iii) deviations from Franck–Condon predictions for most v^+ levels are large (up to 30%–70%), which, in the absence of other interactions, should be easily detected; (iv) the $(3+1)$-REMPI scheme should be most sensitive to orbital evolution and Cooper minimum effects, since the kinetic energy of the photoelectron is located within the range of Cooper minimum [e.g., see Fig. 4(a)]. Figure 6 shows plots of our vibrationally resolved asymmetry parameters for photoionization of the $v' = 3$ levels of the resonant state. The photoelectron angular distributions do not have as strong non-Franck–Condon effects as in the vibrational branching ratios (Fig. 5). Note that this is not so for a shape or autoionizing resonance, but derives here from the photoelectron kinetic energies within the region of the Cooper minimum. The $5\sigma \rightarrow k\sigma$ contribution, which is more Franck–Condon (see Figs. 2 and 4), therefore dominates in both $\Delta v = 0$ and $\Delta v \neq 0$ transitions.

B. Ground state photoionization

We show our calculated cross sections for 3σ photoionization leading to the $a\,^4\Sigma^-$ and $A\,^2\Sigma^-$ ions in Fig. 7(a) and for 1π photoionization of the $X\,^2\Pi$ ionic state in Fig. 7(b) at the equilibrium internuclear distance $R_e = 1.9616a_0$. The difference of spectral profiles between Figs. 7(a) and 7(b)

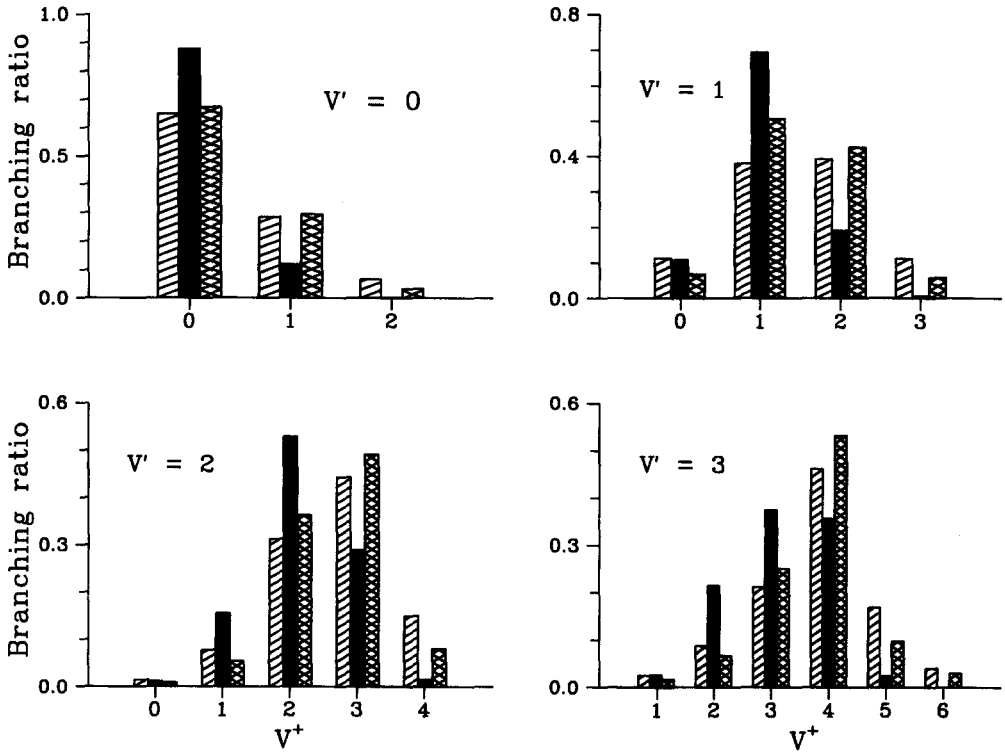

FIG. 5. Calculated vibrational branching ratios for NH $3\,^3\Pi(v'=0\text{–}3)$ $(3+1)$ REMPI. The one photon energies for the $v'=0$–3 frame are 3.593, 3.712, 3.826, and 3.936 eV, respectively. Franck–Condon ratio (solid bar); full length form (slashed bar); full velocity form (cross-hatched bar). In each frame, the branching ratios were obtained with a normalization such that a sum over v^+ for each level v' gives unity.

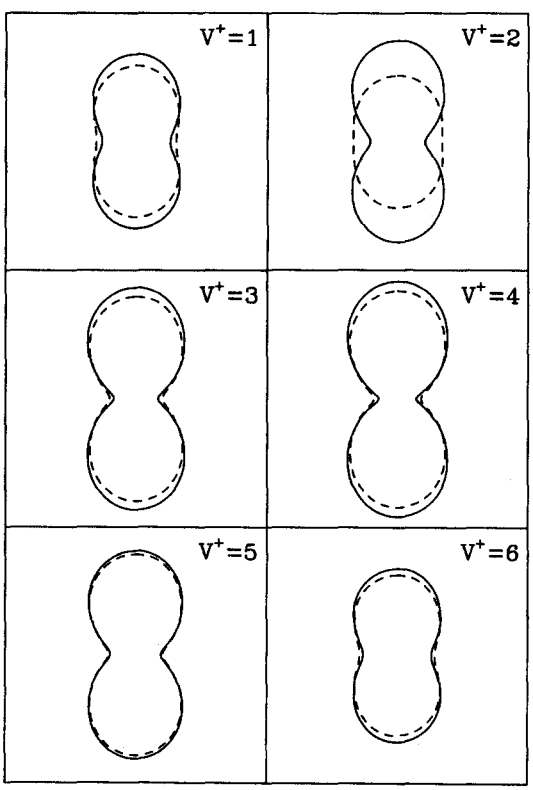

FIG. 6. Calculated vibrationally resolved photoelectron angular distributions for REMPI of NH via the $v'=3$ level of the $3\,^3\Pi$ state for different v^+ levels of the $X\,^2\Pi$ ion. Dipole length form, solid curve; dipole velocity form, dashed curve.

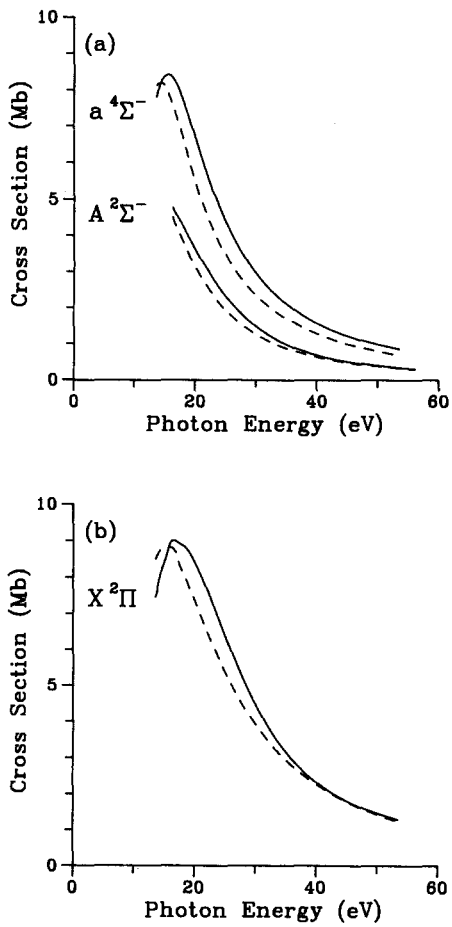

FIG. 7. Calculated photoionization cross sections for producing (a) the $a\,^4\Sigma^-$ and $A\,^2\Sigma^-$ states of NH^+ and (b) the $X\,^2\Pi$ state of NH^+. Dipole length form, solid curve; dipole velocity form, dashed curve.

can be attributed to the different origins of the 3σ and 1π valence orbitals, i.e., the 3σ molecular orbital consists mainly of the nitrogen $2p_z$ atomic orbital, and the 1π orbital consists of "nonbonding" nitrogen $2p_x$ and $2p_y$ atomic orbitals. The ratio of the $a\,^4\Sigma^-$ and $A\,^2\Sigma^-$ cross sections [Fig. 7(a)] is quite close to the statistical ratio 2:1, with a few percent deviation over the entire kinetic energy range. The calculated asymmetry parameters β are shown in Fig. 8 for the 3σ [Figs. 8(a) and 8(b)] and 1π [Fig. 8(c)] orbitals. It is obvious that the asymmetry parameters and cross sections are similar to those of the nitrogen and oxygen atoms.[47] Generally, the photoionization dynamics of NH ground state photoionization mirrors that of the other first-row hydrides OH and CH.[48]

IV. CONCLUSION

In this paper, we have studied vibrationally resolved photoionization dynamics of the $3\,^3\Pi$ Rydberg state of NH leading to the $X\,^2\Pi$ ionic state, assuming a one-color (3 + 1) REMPI scheme. The present calculations predict a strong non-Franck–Condon effect in the resulting vibrational branching ratios. This effect is due to rapid evolution of the Rydberg orbital with internuclear distance, coupled with a $3p \rightarrow k\pi$ Cooper minimum which occurs at small R near the united atom. Future work will examine the rotational ion distributions resulting from REMPI of NH.[45,46] This is of particular interest since, owing to the occurrence of a Cooper minimum and the dominance of a single partial wave in the continuum in their vicinity (e.g., s wave), it may be possible to produce rotationally state-selected molecular ions by tuning the energy of the ionizing photon though the minimum.[49] Additionally, we have studied the photoionization of the 3σ and 1π valence orbitals leading to the three lowest electronic states of the ion by employing multiplet-specific ion potentials.

ACKNOWLEDGMENTS

This work was supported by grants from the National Science Foundation (CHE-8521391), Air Force Office of Scientific Research (Contract No. 87-0039), and the Office of Health and Environmental Research of the U. S. Department of Energy (DE-FG03-87ER60513). We also acknowledge use of resources of the San Diego SuperComputer Center, which is supported by the National Science Foundation, and resources of the Jet Propulsion Laboratory/Caltech Cray X-MP.

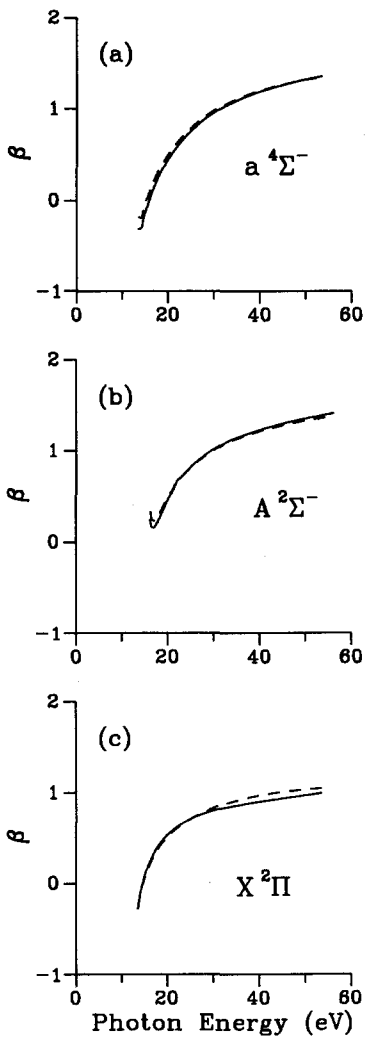

FIG. 8. Calculated asymmetry parameters β for (a) $a\,^4\Sigma^-$; (b) $A\,^2\Sigma^-$; and (c) $X\,^2\Pi$ states of NH^+. Other designations are the same as in Fig. 7.

[1] R. N. Compton and J. C. Miller, in *Laser Applications in Physical Chemistry*, edited by D. K. Evans (Dekker, New York, 1988), Sec. 4.
[2] P. M. Dehmer, J. L. Dehmer, and S. T. Pratt, Comments At. Mol. Phys. **19**, 205 (1987).
[3] P. M. Johnson and C. E. Otis, Annu. Rev. Phys. Chem. **32**, 139 (1981).
[4] J. W. Hudgens, in *Advances in Multiphoton Processes and Spectroscopy*, edited by S. H. Lin (World Scientific, Singapore, 1988), Vol. 4.
[5] W. A. Chupka, J. Chem. Phys. **87**, 1488 (1987).
[6] G. C. Neiman and S. D. Colson, J. Chem. Phys. **68**, 5656 (1978); J. H. Glownia, S. J. Riley, S. D. Colson, and G. C. Nieman, *ibid.* **73**, 4296 (1980).
[7] R. D. Kenner, F. Rohrer, and F. Stuhl, J. Chem. Phys. **86**, 2036 (1987).
[8] F. Rohrer and F. Stuhl, J. Chem. Phys. **88**, 4788 (1988); B. R. Foy, M. P. Casassa, J. C. Stephenson, and D. S. King, *ibid.* **89**, 608 (1988); M. H. Alexander, H. J. Werner, and P. J. Dagdigian, *ibid.* **89**, 1388 (1988).
[9] T. A. Spiglanin and D. W. Chandler, J. Chem. Phys. **87**, 1577 (1987).
[10] J. Chen, E. Quiñones, and P. J. Dagdigian, J. Chem. Phys. **90**, 7603 (1989).
[11] A. R. Whyte and L. F. Phillips, Chem. Phys. Lett. **102**, 451 (1988); A. M. Dean, M.-S. Chou, and D. Stern, Int. J. Chem. Kinetics **16**, 633 (1984); C. F. Melius and J. S. Binkley, ACS Symp. Ser. **249**, 103 (1984).
[12] M. M. Litvak and E. N. Rodriguez Kuiper, Astrophys. J. **253**, 622 (1982).
[13] S. B. Yorka, Astron. J. **88**, 1816 (1983).
[14] R. E. Roach, Astrophys. J. **89**, 99 (1939).
[15] J. A. Stephens and V. McKoy, Phys. Rev. Lett. **62**, 889 (1989).
[16] H. Rudolph, J. A. Stephens, V. McKoy, and M. T. Lee, J. Chem. Phys. **91**, 1374 (1989).
[17] R. R. Lucchese, G. Raseev, and V. McKoy, Phys. Rev. A **25**, 2572 (1982).
[18] R. R. Lucchese, K. Takatsuka, and V. McKoy, Phys. Rep. **131**, 147 (1986).
[19] H. P. D. Liu and G. Verhaegen, J. Chem. Phys. **53**, 735 (1970).
[20] S. N. Foner and R. L. Hudson, J. Chem. Phys. **45**, 40 (1966).
[21] R. Rosmus and W. Meyer, J. Chem. Phys. **66**, 13 (1977).
[22] M. Braunstein, V. Mckoy, and M. E. Smith, J. Chem. Phys. **90**, 3931 (1989).
[23] R. Colin and A. E. Douglas, Can. J. Phys. **46**, 61 (1968).
[24] T. H. Dunning, J. Chem. Phys. **53**, 2823 (1970); **55**, 3958 (1971).
[25] W. J. Hunt and W. A. Goddard, Chem. Phys. Lett. **3**, 414 (1967).
[26] E. M. Goldfield and K. P. Kirby, J. Chem. Phys. **87**, 3986 (1987).
[27] D. R. Yarkony, J. Chem. Phys. **91**, 4745 (1989).

[28] H. P. D. Liu and G. Verhaegen, Int. J. Quantum Chem. **5**, 103 (1971).
[29] R. S. Mulliken, Rev. Mod. Phys. **4**, 1 (1932).
[30] C. E. Moore, *Atomic Energy Levels, as Derived from the Analyses of Optical Spectra* (U. S. GPO, Washington, D. C., 1971), Vol. 1.
[31] H. Lefebvre-Brion and R. W. Field, *Perturbations in the Spectra of Diatomic Molecules* (Academic, Orlando, 1986), Chap. 4.
[32] R. S. Mulliken, Acc. Chem. Res. **9**, 7 (1976).
[33] H. Lefebvre-Brion, in *Molecules in Physics, Chemistry, and Biology*, edited by Jean Maruani (Reidel, Dordrecht, Holland, 1988), Vol. 2.
[34] J. A. Stephens and V. McKoy, J. Chem. Phys. **93**, 7863 (1990).
[35] Ch. Jungen and O. Atabek, J. Chem. Phys. **66**, 5584 (1977).
[36] U. Fano and J. W. Cooper, Rev. Mod. Phys. **40**, 441 (1968).
[37] J. Cooper, Phys. Rev. **128**, 681 (1962).
[38] A. Z. Msezane and S. T. Manson, Phys. Rev. Lett. **48**, 473 (1982).
[39] S. T. Manson, Phys. Rev. A **31**, 3698 (1985).
[40] T. A. Carlson, M. O. Krause, W. A. Svensson, P. Gerard, F. A. Grimm, T. A. Whitley, and B. P. Pullen, Z. Phys. D **2**, 309 (1986).
[41] A. F. Starace, in *Handbuch der Physik*, edited by M. Mehlhorn (Springer, Berlin, 1982), Vol. 31, pp. 1–121.
[42] R. R. Lucchese and V. McKoy, J. Phys. B **14**, 1629 (1981).
[43] P. M. Dittman, D. Dill, and J. L. Dehmer, J. Chem. Phys. **76**, 5703 (1982).
[44] G. Raseev, H. Lerouzo, and H. Lefebvre-Brion, J. Chem. Phys. **72**, 5701 (1980).
[45] K. Wang and V. McKoy (to be published).
[46] K. Wang, J. A. Stephens, H. Rudolph, and V. McKoy (to be published).
[47] S. T. Manson, D. J. Kennedy, A. F. Starace, and D. Dill, Planet. Space Sci. **22**, 1535 (1974).
[48] J. A. Stephens and V. McKoy, J. Chem. Phys. **88**, 1737 (1988); M.-T. Lee, J. A. Stephens, and V. McKoy, *ibid.* **92**, 536 (1990).
[49] H. Rudolph and V. McKoy, J. Chem. Phys. **91**, 7995 (1989); J. Chem. Phys. (accepted for publication).